Effects of Tropospheric Height and Wind Speed on Solar Power Generation: Energy Exploration Above ground Level

Stephen Ndubuisi Nnamchi[1*], Faith Natukunda[2], Silagi Wanambwa[3], Enos Bahati Musiime[4], Richard Tukamuhebwa[5], Titus Wanazusi[6], Emmanuel Ogwal[7]

1. Department of Mechanical Engineering, SEAS, Kampala International University, P.O. Box 20000, Kampala, Uganda, stephen.nnamchi@kiu.ac.ug, ORCID: https://orcid.org/ 0000-0002-6368-2913.
2. Department of Mechanical and Industrial Engineering, Mbarara University of Science and Technology, fnatukunda@must.ac.ug, ORCID: https://orcid.org/ 0000-0003-0299-1381
3. Department of Energy, Mineral and Petroleum Studies, Mbarara University of Science and Technology, swanambwa@must.ac.ug, ORCID: https://orcid.org/ 0000-0002-8850-6051
4. Department of Civil Engineering, SEAS, Kampala International University, P.O. Box 20000, Kampala, Uganda, enos.musiime@kiu.ac.ug, ORCID; https://orcid.org/0000-0002-6357-5325
5. Department of Mechanical Engineering, SEAS, Kampala International University, P.O. Box 20000, Kampala, Uganda, tukamuhebwa@kiu.ac.ug, ORCID; https://orcid.org/0000-0002-9535-5386
6. Department of Mechanical Engineering, SEAS, Kampala International University, P.O. Box 20000, Kampala, Uganda, titus.wanazusi@kiu.ac.ug, ORCID; 0000-0003-1334-9503
7. Department of Electrical, Telecommunication and Computer Engineering, SEAS, Kampala International University, P.O. Box 20000, Kampala, Uganda, emmanuel.ogwal@kiu.ac.ug, ORCID; https://orcid.org/0000-0001-7962-0488

ABSTRACT

Terrestrial and extraterrestrial factors hinder the exploitation of solar power using a ground platform. This paper is concerned with the generation of solar power above ground level. This paper employs modeling and simulations coupled with experimentation to establish a functional relationship between the percentage of solar power gain, tropospheric height and wind speed. The natural wind flow equation established a linear relationship between tropospheric height and wind speed, between tropospheric height and the percentage of solar power gain. It is evident that an insignificant percentage of solar power gain (≈2 %) corresponded to 1000 m above ground level; the tropospheric height of 8100 m recorded 20 % of solar power gain. Furthermore, wind speeds of 0 to 33 ms^{-1}/distance (1000 m) correspond to ground level and tropospheric height of about 8100 m. However, there is a prospect of achieving more percentage of solar power gain by applying high-altitude platforms. The results obtained apply to other study areas having elevations below or equal to 1100 m, it serves as a guide in the estimation of the percentage of solar power gain by the virtue of tropospheric height and wind speed.

Keywords: Percentage of solar power gain, wind speed, tropospheric height, modeling and simulation.

1.0 INTRODUCTION

The socio-economic development of regions and sub-regions depends on the ability of the regions and sub-regions to have self-sustained clean energy generation. Nowadays, it is imperative to explore and exploit

clean energy resources of regions and sub-regions in order to have sustainable socio-economic growth in the regions (Tucho, 2020; Rublev et al, 2021). Pertinently, Owusu and Asumadu-Sarkodie (2016) assert the need for energy and its related services to satisfy social and economic development, welfare and health in different regions of the world is perpetually on the increase. Among the renewable energy resources available for satisfying the global energy demand, solar-photovoltaic energy resources and technology remain the most accessible, affordable and sustainable clean energy sources (Majid, 2020; Bogdanov et al, 2021; Maka and Alabid, 2022).

Hence, solar panels are more likely to be efficient at high altitudes because solar radiation increases with altitude in the atmosphere (about 8 – 12 %/304.8 m) and atmospheric temperature is low with increasing wind speed to induce fast cooling of the solar panels due to decrease in air molecules, emissions and air temperature. Maximizing radiation and minimizing temperature leads to optimum power generation in solar panels (Chandra, 2018), these conditions are favored by high altitude (Somadi, 2016; Bhattacharya, 2014). Moreover, the intensity of solar irradiance on a solar panel hinges on the zenith angle and the relative distance of the sun to the earth (Zhang et al, 2021). Blumthaler et al (1997) observed the magnitude of increase in irradiance with altitude; the daily total of global irradiance ranged between 8%±2% per 1000 m (total irradiance), whereas UVA irradiance ranged between 9%±2% per 1000 m in a clear sky condition. Furthermore, an increase or decrease in the distance between the sun and earth relative to the mean distance between the sun and earth induces high or low solar radiation on a horizontal surface, respectively (Pielke Sr, 2013). In addition, it is phenomenal that whenever the sun is overhead, the earth experiences the maximum intensity of solar radiation, thus, the solar panel outputs peak power (Zakšek, 2005; Amaya, 2019).

Uncertainly, Amusan and Igbudu (2014) assert that height has no significant impact on the PV power output. The methodology for investigating the impact of height was deficient in the control experiment, there was no second panel placed on the ground level to simultaneously record power at the ground level. They varied the height of PV from 0 to 4.68 m and recorded ideal power every 15 minutes, not considering that insolation is not constant. Thus, there should have been an unshaded control panel placed on the ground to simultaneously record the ideal power at zero level and the second panel to track ideal power at any given height, this technique would have demystified or debunked their assertion.

Contrarily, in characterizing the influence of installation height and a green roof on PV performance of ground platforms, Osman et al (2016) emphasize that a lower height (about 0.5 m above a roof) increases PV performance by 1 %, and 2% by a green roof, whereas both increases the PV performance by 2.8%. This is a micro power gain compared to macro power gain in the high altitudes (above the troposphere), however, the height of the green roof is uncertain, thus, neglecting the impact of height on the power gain. Panjwani and Narejo (2014) observed that by placing a panel at an altitude/height of 90 ft /27.432 m power accession of 7-12 % was gained. This result is authenticated by a ground control experiment running simultaneously with an elevated experiment. At higher altitudes, we get more direct irradiation and little diffused radiation, which increases the output power because the inhibiting factors are minimal, however, the lifespan of the photovoltaic panel is reduced and the cost of installation is high (jntechenergy, 2022). Asgharzadeh (2018) showed that there is a corresponding gain in PV output power below the unspecified saturation height, subsequently, height does not impact the PV output power. However, this conclusion is not supporting the development of high-altitude platforms, HAP, which explore energy beyond the tropospheric or saturation height. Few works support that high altitude engenders more photovoltaic output power (Aglietti et al, 2008; Panjwani and Narejo, 2014). Alrwashdeh (2018) affirms that optimizing the height of the tower supporting a solar panel facilitates greater power production. Chitturi et al (2018) showed that at a height of 1764 m that the efficiency of solar panels increases by 42 % compared to the ones placed at a height of 612 m above sea level. Besides the impact of height, a previous study (Shastry and Arunachala, 2020;) supports that cooling of photovoltaic panels enhances their output power.

According to Sharaf et al (2022) cooling could be active (Hassan et al., 2021; Deokar et al, 2021; Dwivedi, 2020), passive (Ramkiran et al., 2021; Rakino et al., 2019, Wu and Xiong, 2014), phase change material, PCM (Sahu et al., 2021; Hassan et al, 2014; Seto et al., 2021) and additive PCM (Mahdi et al., 2021; Luo, 2017; Atkin and Farid, 2015) aimed at increasing photovoltaic output power. Significantly, cold air is found in the higher atmosphere boosting the performance of HAP. Due to the abundance of air within and beyond tropospheric Height, the present study will be limited to the passive cooling of photovoltaic panels using natural air.

In order to utilize the solar energy available in the high atmosphere, it is necessary to have a high-altitude platform (HAP) or high-altitude aerostatic platform to support appropriate photovoltaic panels (Chitturi et al, 2018; Aglietti et al, 2008; Gupta et al, 2019) could be heavier-than-air (fixed wing airplane) or lighter-than-air (Balloons, Airships and Propulsion Assisted High-Altitude Platform - PAHAP). Pertinently, this HAP could access solar power to the tune of 25 km, which is above the tropospheric height the present work is studying. Based on the literature considered, there is hardly any that has shown progressive power gain as the altitude increases. With the exception of Panjwani and Narejo (2014) most works in literature, employed uncontrolled experiments to measure only near-ground parameters (power and power gain), whereas some used HAP to measure power in the troposphere and beyond. However, the present work employs modeling and simulation of airflow and practical measurement of ideal power to establish the progressive solar power gain up to an altitude of 9200 m and air speed of 42 m/s according to radiosonde data (Kräuchi and Philipona, 2016).

The Navier Strokes equation applies to three-dimensional (3-D) modeling and simulation of fluid potential in a flowing system (Loria, 2020; Ahammad et al., 2019; Oko and Nnamchi, 2013). Inclusively, Nnamchi et al (2021) demonstrated the practical application of the Navier Strokes equation in solar-biomass drying. Phenomenally, the present work extends the application of the Navier Stokes equation to the modeling and simulation of tropospheric wind speeds and tropospheric solar power gain in photovoltaic panels. The Navier Stokes equation for fluid flow applies to solar power gain as this potential replaces vertical wind speed in a boundary value problem emanating from the Navier Stokes equation. The contour analysis of the percentage of solar power gain demonstrates the impact of tropospheric height and wind speed on the percentage of solar power gain. The application of validated model results becomes inevitable and veritable when the measurement is difficult in a remote atmosphere close to the sun.

Therefore, the present work via controlled experiments, modeling and simulations establishes a practical relationship; between the tropospheric height and wind speed, between the tropospheric height and percentage of solar power gain, and further presents effective solar power gain as a function of tropospheric height and wind speed from the ground level to prospective altitude, which supports progressive solar energy exploitation above the ground level.

2.0 MATERIALS AND METHOD

This paper employs both analysis and experiment in order to realize the objectives of this work as stated in Section 1. Model formulation and simulations portray the analysis of wind flow and percentage of solar power gain in the study areas.

2.1 *Map of the study area*

The study (practical measurement) was carried out at the Western Campus of Kampala International University, Uganda. Fig.1 shows the map of the study areas. However, the analysis covered the four regions of Uganda; the Northern region (NR), the Eastern Region (ER), the Central Region (CR) and the Western

Region (WR) at elevations of 1073, 1143, 1200 and 1473 m, respectively. Uganda is a Sub-Sahara country situated in East Africa, Landlocked by South Sudan in the north, Kenya in the east, the Democratic Republic of the Congo in the west, and Tanzania/Rwanda in the south. Uganda occupies a total land mass of 241559 ($sq.km$); the NR, ER and WR cover 82099, 39479, 61403 and 55277 ($sq.km$), respectively. The major power supply to the national grid is via hydropower generation, 743 MW, which is complemented by ground-level solar power generation in NR (none), ER (Tororo plant; 32000 panels with a generation capacity of 10 MW, Busitema plant with a generation capacity of 4MW; Mayuge plant 30600 panels with a generation capacity of and Soroti plant; 32680 panels with a generation capacity of 10MW), CR (Kabulasoke plant; 68000 solar panels with a generation capacity of 20 MW) Nnamchi et al (2022) and WR (none). Thus, solar power generated from the two regions (ER and CR) is approximately 50 MW. The Western Regions has no ground platform partly due to the sloping nature of the region, low average wind speed (5.8 km/h) and least irradiance according to Mundu et al (2022). Despite these disadvantageous factors, the present work looks into the prospect of exploring solar power above ground level, in this region and other regions, and the introduction of high-altitude platforms in Uganda.

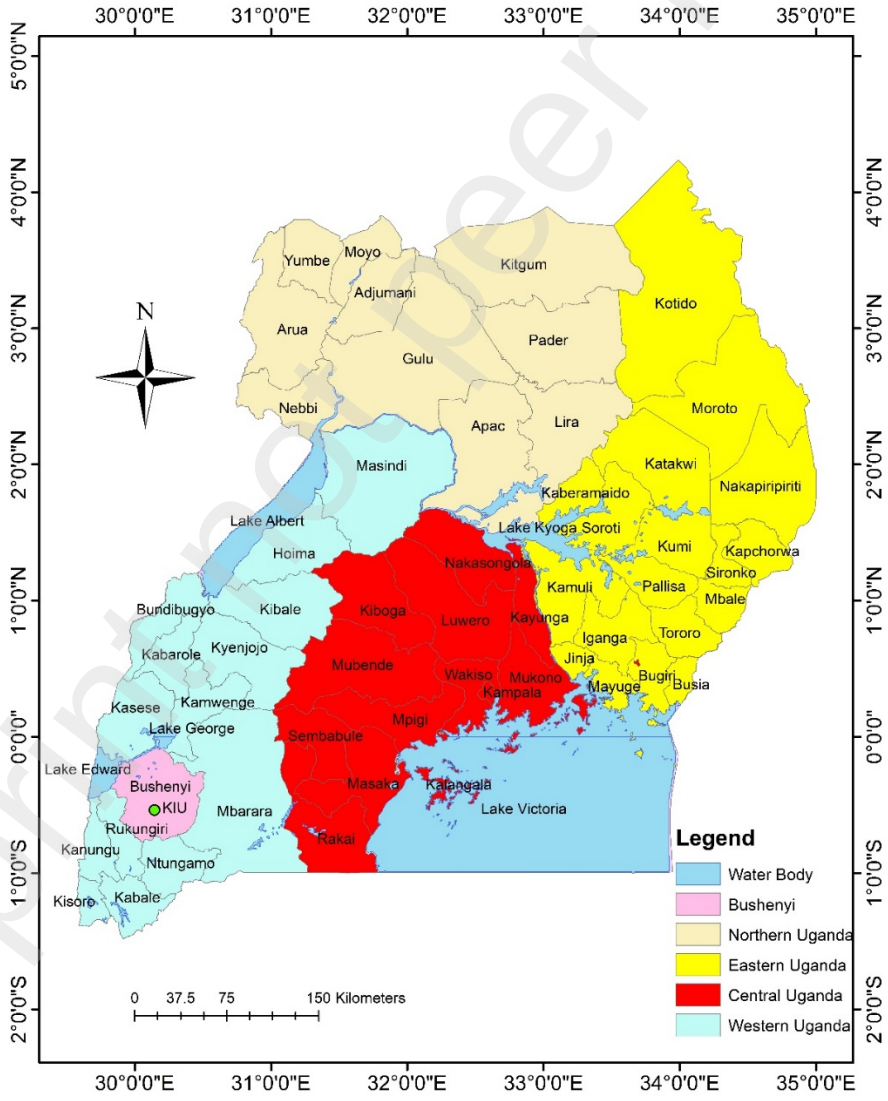

Fig. 1 Map of the study areas

2.2 *Experiments*

Three elevated stations within the Western Campus of Kampala International University were chosen; the Engineering Complex (station 1), the Hostel Complex (station 2) and the Library complex (station 3). The depressed or reference station is the Convocation ground under construction. Two photovoltaic panels (Mira Cozy PV modules; MC010W-18P) were used to measure ideal electric power; the short circuit current (SC) and open circuit voltage (OC) with the aid of Pocket Digital Multi-Meters (MASTECH M830BZ, IEC 61010-1, ±1.2%). By connecting the terminals of the solar panel and the multi-meter, a consecutive measurement of direct current (DC, SC) and direct voltage (DV, OC) was feasible. For the purposes of tracking the percentage of solar power gain, a solar panel was kept at elevated height, whereas the second solar panel was placed in an unshaded and depressed position. Readings were simultaneously taken at an interval of 15 minutes when the sun is on noonday (between 1:00 to 2:00 PM). A Surveying Steel tape (BESTIR 01702, 50 m, ±0.03 inch) was used to measure the height of the elevated position from the unshaded and depressed position. The vertical height was measured directly, the sloped height was determined by measuring the slope length, a protractor (Helix H01, ±0.25°) was used to determine the slope angle and right-angle geometry was used to calculate the corresponding sloping height. Thus, the true vertical height is the summation of sloping height and the vertical height of the structures used to place the elevated solar panel. The experiment was observed for six months only on noonday for the purpose of having appreciable and regular readings. The experiment was observed every 15-minute interval, the DC current and voltage were measured and the average values were taken. The percentage of power gain was determined by computing the difference between elevated and depressed solar panel electric powers. A simple multiple linear regression model percentage of power gain against tropospheric height and wind velocity was developed. The measured percentage of power gain validates the simulated one. The pictures of the experimental setup are shown in Figure 1. The practical wind speed was gotten from radiosonde data after subtracting the elevation of the study areas from the altitude corresponding to the first peak height of the wind speed about 9200 m (≡ 42 ms^{-1}/distance 1000 m) in Fig 2. The near-ground measured average wind speed data obtained from radiosonde (Kräuchi and Philipona, 2016) was compared with meteorological data (Accueather.com) ranging from 2.22 – 3.61 m/s.

Top view of Engineering Complex

2a. Engineering Complex

2b. Hostel Complex

2c. Library Complex

Ground level (Datum)

Top view Hostel Complex

Ground level (Datum)

Top view of Library Complex

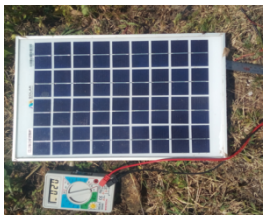

Ground level (Datum)

Fig. 2 Measurement sites

176

177 2.3 *Model and Numerical Formulation of wind flow*

178 Wind flows are formulated in three dimensions (x,y,z) like any other fluids. Navier Stokes model describes
179 a fluid flow in three dimensions, 3-D (Radwan et al., 2021). Excluding physical forces gravity force, GF

(Rapp, 2016), pressure gradient force, PGF (Taha and Gonzalez, 2022) and Coriolis force, CF (Lee, 2017), the flow describes natural wind flow (NWF), whereas the presence of the extrinsic physical forces makes the flow to be forced wind flow (FWF). The natural wind flow equation (NWFE) comprises a local acceleration of the fluid, convective fluid flow and diffusive terms in Eq.(1a)

$$\frac{\partial u_x}{\partial t}+u_x\frac{\partial u_x}{\partial x}+u_y\frac{\partial u_x}{\partial y}+u_z\frac{\partial u_x}{\partial z}=\upsilon\left(\frac{\partial^2 u_x}{\partial x^2}+\frac{\partial^2 u_x}{\partial y^2}+\frac{\partial^2 u_x}{\partial z^2}\right)\quad \exists \quad \upsilon=\frac{\mu}{\rho} \tag{1a}$$

where $u_x(m/s)$ is the component wind velocity in the x-direction, $u_y(m/s)$ is the component wind velocity in the y-direction, $u_z(m/s)$ is the component wind velocity in the z-direction, $t(s)$ is the time, $\mu(kg/ms)$ is the dynamic viscosity of the wind, $\rho(kg/m^3)$ is the density of the wind, $\upsilon(m^2/s)$ is the kinematic viscosity of the wind.

Similarly, NWFE in the y-direction is presented in Eq.(2a) as

$$\frac{\partial u_y}{\partial t}+u_x\frac{\partial u_y}{\partial x}+u_y\frac{\partial u_y}{\partial y}+u_z\frac{\partial u_y}{\partial z}=\frac{\mu}{\rho}\left(\frac{\partial^2 u_y}{\partial x^2}+\frac{\partial^2 u_y}{\partial y^2}+\frac{\partial^2 u_y}{\partial z^2}\right)\quad \exists \quad \upsilon=\frac{\mu}{\rho} \tag{2a}$$

where $u_y(m/s)$ is the component wind velocity in the y-direction. NWFE in the z-direction is presented in Eq.(3a) as

$$\frac{\partial u_z}{\partial t}+u_x\frac{\partial u_z}{\partial x}+u_y\frac{\partial u_z}{\partial y}+u_z\frac{\partial u_z}{\partial z}=\frac{\mu}{\rho}\left(\frac{\partial^2 u_z}{\partial x^2}+\frac{\partial^2 u_z}{\partial y^2}+\frac{\partial^2 u_z}{\partial z^2}\right)\quad \exists \quad \upsilon=\frac{\mu}{\rho} \tag{3a}$$

where $u_z(m/s)$ is the component wind velocity in the z-direction.

Imposing steady state condition on Eqs.(1a-3a), Eigenvector models are developed in Eqs.(1b-3b), then, the steady-state of Eq.(1a) is given in Eq.(1b) as

$$u_x\frac{\partial u_x}{\partial x}+u_y\frac{\partial u_x}{\partial y}+u_z\frac{\partial u_x}{\partial z}=\upsilon\left(\frac{\partial^2 u_x}{\partial x^2}+\frac{\partial^2 u_x}{\partial y^2}+\frac{\partial^2 u_x}{\partial z^2}\right)\quad \exists \quad \upsilon=\frac{\mu}{\rho} \tag{1b}$$

Similarly, the steady-state Eigenvector of Eq.(2a) is expressed in Eq.(2b) as

$$u_x\frac{\partial u_y}{\partial x}+u_y\frac{\partial u_y}{\partial y}+u_z\frac{\partial u_y}{\partial z}=\frac{\mu}{\rho}\left(\frac{\partial^2 u_y}{\partial x^2}+\frac{\partial^2 u_y}{\partial y^2}+\frac{\partial^2 u_y}{\partial z^2}\right)\quad \exists \quad \upsilon=\frac{\mu}{\rho} \tag{2b}$$

In the same vein, the steady-state Eigenvector of Eq.(3a) is written in Eq.(3b) as

$$u_x\frac{\partial u_z}{\partial x}+u_y\frac{\partial u_z}{\partial y}+u_z\frac{\partial u_z}{\partial z}=\frac{\mu}{\rho}\left(\frac{\partial^2 u_z}{\partial x^2}+\frac{\partial^2 u_z}{\partial y^2}+\frac{\partial^2 u_z}{\partial z^2}\right)\quad \exists \quad \upsilon=\frac{\mu}{\rho} \tag{3b}$$

The resultant velocity, $u(m/s)$ is expressed by the component velocities of the wind in Eq.(4)

$$u^2=u_x^2+u_y^2+u_z^2\Rightarrow u=\left(u_x^2+u_y^2+u_z^2\right)^{0.5} \tag{4}$$

The linear relationship between the component wind velocities and step changes is approximated in Eq.(5) as

$$\frac{u_x}{u_y} \approx \frac{\Delta x}{\Delta y}, \frac{u_x}{u_z} \approx \frac{\Delta x}{\Delta z} \Rightarrow u_x = \frac{\Delta x}{\Delta y} u_y, \; u_x = \frac{\Delta x}{\Delta z} u_z$$
$$\frac{u_y}{u_x} \approx \frac{\Delta y}{\Delta x}, \frac{u_y}{u_z} \approx \frac{\Delta y}{\Delta z} \Rightarrow u_y = \frac{\Delta y}{\Delta x} u_x, \; u_y = \frac{\Delta y}{\Delta z} u_z \quad (5)$$
$$\frac{u_z}{u_x} \approx \frac{\Delta z}{\Delta x}, \frac{u_z}{u_y} \approx \frac{\Delta z}{\Delta y} \Rightarrow u_z = \frac{\Delta z}{\Delta x} u_x, \; u_z = \frac{\Delta z}{\Delta y} u_y$$

Substituting Eq.(5) into Eqs.(1b-3b) yields the modified NWFE in Eqs.(6-8) respectively with one dependent variable.

$$u_x\left(\frac{\partial u_x}{\partial x} + \left(\frac{\Delta y}{\Delta x}\right)\frac{\partial u_x}{\partial y} + \left(\frac{\Delta z}{\Delta x}\right)\frac{\partial u_x}{\partial z}\right) = \upsilon\left(\frac{\partial^2 u_x}{\partial x^2} + \frac{\partial^2 u_x}{\partial y^2} + \frac{\partial^2 u_x}{\partial z^2}\right) \quad (6)$$

and

$$u_y\left(\left(\frac{\Delta x}{\Delta y}\right)\frac{\partial u_y}{\partial x} + \frac{\partial u_y}{\partial y} + \left(\frac{\Delta z}{\Delta y}\right)\frac{\partial u_y}{\partial z}\right) = \upsilon\left(\frac{\partial^2 u_y}{\partial x^2} + \frac{\partial^2 u_y}{\partial y^2} + \frac{\partial^2 u_y}{\partial z^2}\right) \quad (7)$$

and

$$u_z\left(\left(\frac{\Delta x}{\Delta z}\right)\frac{\partial u_z}{\partial x} + \left(\frac{\Delta y}{\Delta z}\right)\frac{\partial u_z}{\partial y} + \frac{\partial u_z}{\partial z}\right) = \upsilon\left(\frac{\partial^2 u_z}{\partial x^2} + \frac{\partial^2 u_z}{\partial y^2} + \frac{\partial^2 u_z}{\partial z^2}\right) \quad (8)$$

Considering vertical wind flow; Eqs. (6 and 7) vanish as u_x and u_y become zero. Also, wind flow gradient in z-direction becomes zero ($\partial / \partial z = 0$), thus, Eq.8) reduces to Eq.(9a)

$$u_z\left(\left(\frac{\Delta x}{\Delta z}\right)\frac{\partial u_z}{\partial x} + \left(\frac{\Delta y}{\Delta z}\right)\frac{\partial u_z}{\partial y}\right) = \upsilon\left(\frac{\partial^2 u_z}{\partial x^2} + \frac{\partial^2 u_z}{\partial y^2}\right) \quad (9a)$$

The dependent variable u_z in Eq. (9a) is substituted with percentage power gain, $p_z(\%)$ in Eq. (9b)

$$u_z\left(\left(\frac{\Delta x}{\Delta z}\right)\frac{\partial p_z}{\partial x} + \left(\frac{\Delta y}{\Delta z}\right)\frac{\partial p_z}{\partial y}\right) = \upsilon\left(\frac{\partial^2 p_z}{\partial x^2} + \frac{\partial^2 p_z}{\partial y^2}\right) \quad \exists \quad p_z = \frac{\left(P_{z,top} - P_{z,base}\right)}{P_{z,base}} \quad (9b)$$

where $P_{z,top}(W)$ is the power above the ground level and $P_{z,base}(W)$ is the power at the ground level.

2.3.1 Numerical solutions of the NWFE model

The numerical solution is preferred for the ease of realizing the approximate solution of the linear wind flow models in Eq.(9a). The linear equations are composed of differential and nondifferential linear terms. The solution is achieved by discretizing the differential and nondifferential linear terms.

2.3.2 Space discretization of nondifferential linear terms

The discretization of the nondifferential linear terms is shown in Eq.(10)

$$u_z = u_{z,i}^n \quad (10)$$

2.3.3 *Space discretization of differential linear terms*

The implicit and explicit discretization of the differential linear terms are based on their order (first and second) shown in Eq.(11) and Eq.(12) respectively. Center discretization applies at the interior nodes, whereas forward discretization applies at the boundary nodes

$$\frac{\partial u_z}{\partial x}=\theta\frac{u^{n+1}_{z,i+1}-u^{n+1}_{z,i-1}}{2\Delta x}+(1-\theta)\frac{u^{n}_{z,i+1}-u^{n}_{z,i-1}}{2\Delta x};\qquad \frac{\partial u_z}{\partial y}=\theta\frac{u^{n+1}_{z,i+1}-u^{n+1}_{z,i-1}}{2\Delta y}+(1-\theta)\frac{u^{n}_{z,i+1}-u^{n}_{z,i-1}}{2\Delta y} \tag{11}$$

and

$$\frac{\partial^2 u_z}{\partial x^2}=\theta\frac{u^{n+1}_{z,i+1}-2u^{n+1}_{z,i}+u^{n+1}_{z,i-1}}{(\Delta x)^2}+(1-\theta)\frac{u^{n}_{z,i+1}-2u^{n}_{z,i}+u^{n}_{z,i-1}}{(\Delta x)^2};\qquad \frac{\partial^2 u_z}{\partial y^2}=\theta\frac{u^{n+1}_{z,i+1}-2u^{n+1}_{z,i}+u^{n+1}_{z,i-1}}{(\Delta y)^2}+(1-\theta)\frac{u^{n}_{z,i+1}-2u^{n}_{z,i}+u^{n}_{z,i-1}}{(\Delta y)^2} \tag{12}$$

where θ is the degree of implicitness, the superscript, n denotes future time, whereas the subscript i denotes the discretized nodes.

Substituting Eqs.(10-12) into Eq.(9a) gives the discretized form of the NWFE (GF=0, PGF=0 and CF=0) in the z-direction in Eq.(13)

$$\begin{aligned}&u^{n}_{z,i}\left(\left(\frac{\Delta x}{\Delta z}\right)\left(\theta\frac{u^{n+1}_{z,i+1}-u^{n+1}_{z,i-1}}{2\Delta x}+(1-\theta)\frac{u^{n}_{z,i+1}-u^{n}_{z,i-1}}{2\Delta x}\right)+\left(\frac{\Delta y}{\Delta z}\right)\left(\theta\frac{u^{n+1}_{z,i+1}-u^{n+1}_{z,i-1}}{2\Delta y}+(1-\theta)\frac{u^{n}_{z,i+1}-u^{n}_{z,i-1}}{2\Delta y}\right)\right)\\&=\upsilon\left(\left(\theta\frac{u^{n+1}_{z,i+1}-2u^{n+1}_{z,i}+u^{n+1}_{z,i-1}}{(\Delta x)^2}+(1-\theta)\frac{u^{n}_{z,i+1}-2u^{n}_{z,i}+u^{n}_{z,i-1}}{(\Delta x)^2}\right)+\left(\theta\frac{u^{n+1}_{z,i+1}-2u^{n+1}_{z,i}+u^{n+1}_{z,i-1}}{(\Delta y)^2}+(1-\theta)\frac{u^{n}_{z,i+1}-2u^{n}_{z,i}+u^{n}_{z,i-1}}{(\Delta y)^2}\right)\right)\end{aligned} \tag{13}$$

2.3.4 *Simplification of numerical solution of the NWFE*

The NWFE, Eq.(13) is rearranged according to its implicit and explicit terms in Eq.(14)

$$\begin{aligned}&-\theta\left(1+\xi_{x,i}+\xi_{y,i}\right)u^{n+1}_{z,i-1}+2\theta\left(\xi_{x,i}+\xi_{y,i}\right)u^{n+1}_{z,i}-\theta\left(-1+\xi_{x,i}+\xi_{y,i}\right)u^{n+1}_{z,i+1}=(1-\theta)\left(1+\left(\xi_{x,i}+\xi_{y,i}\right)\right)u^{n}_{z,i-1}\\&-2(1-\theta)\left(\xi_{x,i}+\xi_{y,i}\right)u^{n}_{z,i}+(1-\theta)\left(-1+\left(\xi_{x,i}+\xi_{y,i}\right)\right)u^{n}_{z,i+1}\quad\exists\quad \xi_{x,i}=\frac{\upsilon\Delta z}{(\Delta x)^2u^{n}_{z,i}}\le 0.5\,,\ \xi_{y,i}=\frac{\upsilon\Delta z}{(\Delta y)^2u^{n}_{z,i}}\le 0.5,\\&if\left(\Delta x>\Delta y\right),\quad \xi_{x,i}<\xi_{y,i}\ ;\ if\left(\Delta x=\Delta y\right),\quad \xi_{x,i}=\xi_{y,i}\ ;\ if\left(\Delta x<\Delta y\right),\quad \xi_{x,i}>\xi_{y,i};\quad RHS\equiv f_{z,i}\end{aligned} \tag{14}$$

where $\xi_{x,i}$ is the stability criterion in the x-direction and $\xi_{y,i}$ is the stability criterion in the y-direction. Considering $n=0,\ 1\le i\le N-1$ leads to a diagonal matrix in Eq.(15a-g)

$$\begin{aligned}&-\theta\left(1+\xi_{x,1}+\xi_{y,1}\right)u^{1}_{z,0}+2\theta\left(\xi_{x,1}+\xi_{y,1}\right)u^{1}_{z,1}-\theta\left(-1+\xi_{x,1}+\xi_{y,1}\right)u^{1}_{z,2}=(1-\theta)\left(1+\left(\xi_{x,1}+\xi_{y,1}\right)\right)u^{0}_{z,0}\\&-2(1-\theta)\left(\xi_{x,1}+\xi_{y,1}\right)u^{0}_{z,1}+(1-\theta)\left(-1+\left(\xi_{x,1}+\xi_{y,1}\right)\right)u^{0}_{z,2}\quad\exists\quad \xi_{x,1}=\frac{\upsilon\Delta z}{(\Delta x)^2u^{0}_{z,1}}\le 0.5\,,\ \xi_{y,1}=\frac{\upsilon\Delta z}{(\Delta y)^2u^{0}_{z,1}}\le 0.5,\\&if\left(\Delta x>\Delta y\right),\quad \xi_{x,1}<\xi_{y,1}\ ;\ if\left(\Delta x=\Delta y\right),\quad \xi_{x,1}=\xi_{y,1}\ ;\ if\left(\Delta x<\Delta y\right),\quad \xi_{x,1}>\xi_{y,1};\ RHS\equiv f_{z,1}\,,\\&u^{0}_{z,0}=2u^{0}_{z,1}-u^{0}_{z,2}\,,\ u^{1}_{z,0}-u^{0}_{z,0}\approx\Delta z\,G,\ \Delta z(m),\ G\left(\frac{m/s}{m}\right)\end{aligned} \tag{15a}$$

$$-\theta\left(1+\xi_{x,2}+\xi_{y,2}\right)u^1_{z,1}+2\theta\left(\xi_{x,2}+\xi_{y,2}\right)u^1_{z,2}-\theta\left(-1+\xi_{x,2}+\xi_{y,2}\right)u^1_{z,3}=\left(1-\theta\right)\left(1+\left(\xi_{x,2}+\xi_{y,2}\right)\right)u^0_{z,1}$$
$$-2\left(1-\theta\right)\left(\xi_{x,2}+\xi_{y,2}\right)u^0_{z,2}+\left(1-\theta\right)\left(-1+\left(\xi_{x,2}+\xi_{y,2}\right)\right)u^0_{z,3}\quad\exists\quad\xi_{x,2}=\frac{\upsilon\Delta z}{\left(\Delta x\right)^2u^0_{z,2}}\le 0.5\ ,\ \xi_{y,2}=\frac{\upsilon\Delta z}{\left(\Delta y\right)^2u^0_{z,2}}\le 0.5, \tag{15b}$$
$$if\left(\Delta x>\Delta y\right),\quad\xi_{x,2}<\xi_{y,2}\ ;\ \ if\left(\Delta x=\Delta y\right),\quad\xi_{x,2}=\xi_{y,2}\ ;\ \ if\left(\Delta x<\Delta y\right),\quad\xi_{x,2}>\xi_{y,2};\quad RHS\equiv f_{z,2}$$

$$-\theta\left(1+\xi_{x,3}+\xi_{y,3}\right)u^1_{z,2}+2\theta\left(\xi_{x,3}+\xi_{y,3}\right)u^1_{z,3}-\theta\left(-1+\xi_{x,3}+\xi_{y,3}\right)u^1_{z,4}=\left(1-\theta\right)\left(1+\left(\xi_{x,3}+\xi_{y,3}\right)\right)u^0_{z,2}$$
$$-2\left(1-\theta\right)\left(\xi_{x,3}+\xi_{y,3}\right)u^0_{z,3}+\left(1-\theta\right)\left(-1+\left(\xi_{x,3}+\xi_{y,3}\right)\right)u^0_{z,4}\quad\exists\quad\xi_{x,3}=\frac{\upsilon\Delta z}{\left(\Delta x\right)^2u^0_{z,3}}\le 0.5\ ,\ \xi_{y,3}=\frac{\upsilon\Delta z}{\left(\Delta y\right)^2u^0_{z,3}}\le 0.5, \tag{15c}$$
$$if\left(\Delta x>\Delta y\right),\quad\xi_{x,3}<\xi_{y,3}\ ;\ \ if\left(\Delta x=\Delta y\right),\quad\xi_{x,3}=\xi_{y,3}\ ;\ \ if\left(\Delta x<\Delta y\right),\quad\xi_{x,3}>\xi_{y,3};\quad RHS\equiv f_{z,3}$$

$$\vdots \tag{15d}$$

$$-\theta\left(1+\xi_{x,N-3}+\xi_{y,N-3}\right)u^1_{z,N-4}+2\theta\left(\xi_{x,N-3}+\xi_{y,N-3}\right)u^1_{z,N-3}-\theta\left(-1+\xi_{x,N-3}+\xi_{y,N-3}\right)u^1_{z,N-2}=\left(1-\theta\right)\left(1+\left(\xi_{x,N-3}+\xi_{y,N-3}\right)\right)u^0_{z,N-4}$$
$$-2\left(1-\theta\right)\left(\xi_{x,N-3}+\xi_{y,N-3}\right)u^0_{z,N-3}+\left(1-\theta\right)\left(-1+\left(\xi_{x,N-3}+\xi_{y,N-3}\right)\right)u^0_{z,N-2}\quad\exists\quad\xi_{x,N-3}=\frac{\upsilon\Delta z}{\left(\Delta x\right)^2u^0_{z,N-3}}\le 0.5\ ,\ \xi_{y,N-3}=\frac{\upsilon\Delta z}{\left(\Delta y\right)^2u^0_{z,N-3}}\le 0.5, \tag{15e}$$
$$if\left(\Delta x>\Delta y\right),\quad\xi_{x,N-3}<\xi_{y,N-3}\ ;\ \ if\left(\Delta x=\Delta y\right),\quad\xi_{x,N-3}=\xi_{y,N-3}\ ;\ \ if\left(\Delta x<\Delta y\right),\quad\xi_{x,N-3}>\xi_{y,N-3};\quad RHS\equiv f_{z,N-3}$$

$$-\theta\left(1+\xi_{x,N-2}+\xi_{y,N-2}\right)u^1_{z,N-3}+2\theta\left(\xi_{x,N-2}+\xi_{y,N-2}\right)u^1_{z,N-2}-\theta\left(-1+\xi_{x,N-2}+\xi_{y,N-2}\right)u^1_{z,N-1}=\left(1-\theta\right)\left(1+\left(\xi_{x,N-2}+\xi_{y,N-2}\right)\right)u^0_{z,N-3}$$
$$-2\left(1-\theta\right)\left(\xi_{x,N-2}+\xi_{y,N-2}\right)u^0_{z,N-2}+\left(1-\theta\right)\left(-1+\left(\xi_{x,N-2}+\xi_{y,N-2}\right)\right)u^0_{z,N-1}\quad\exists\quad\xi_{x,N-2}=\frac{\upsilon\Delta z}{\left(\Delta x\right)^2u^0_{z,N-2}}\le 0.5\ ,\ \xi_{y,N-2}=\frac{\upsilon\Delta z}{\left(\Delta y\right)^2u^0_{z,N-2}}\le 0.5, \tag{15f}$$
$$if\left(\Delta x>\Delta y\right),\quad\xi_{x,N-2}<\xi_{y,N-2}\ ;\ \ if\left(\Delta x=\Delta y\right),\quad\xi_{x,N-2}=\xi_{y,N-2}\ ;\ \ if\left(\Delta x<\Delta y\right),\quad\xi_{x,N-2}>\xi_{y,N-2};\quad RHS\equiv f_{z,N-2}$$

$$-\theta\left(1+\xi_{x,N-1}+\xi_{y,N-1}\right)u^1_{z,N-2}+2\theta\left(\xi_{x,N-1}+\xi_{y,N-1}\right)u^1_{z,N-1}-\theta\left(-1+\xi_{x,N-1}+\xi_{y,N-1}\right)u^1_{z,N}=\left(1-\theta\right)\left(1+\left(\xi_{x,N-1}+\xi_{y,N-1}\right)\right)u^0_{z,N}$$
$$-2\left(1-\theta\right)\left(\xi_{x,N-1}+\xi_{y,N-1}\right)u^0_{z,N-1}+\left(1-\theta\right)\left(-1+\left(\xi_{x,N-1}+\xi_{y,N-1}\right)\right)u^0_{z,N}\quad\exists\quad\xi_{x,N-1}=\frac{\upsilon\Delta z}{\left(\Delta x\right)^2u^0_{z,N-1}}\le 0.5\ ,\ \xi_{y,N-1}=\frac{\upsilon\Delta z}{\left(\Delta y\right)^2u^0_{z,N-1}}\le 0.5, \tag{15g}$$
$$if\left(\Delta x>\Delta y\right),\quad\xi_{x,N-1}<\xi_{y,N-1}\ ;\ \ if\left(\Delta x=\Delta y\right),\quad\xi_{x,N-1}=\xi_{y,N-1}\ ;\ \ if\left(\Delta x<\Delta y\right),\quad\xi_{x,N-1}>\xi_{y,N-1};\quad RHS\equiv f_{z,N-1},$$
$$u^0_{z,N}=2u^0_{z,N-1}-u^0_{z,N-2},\ \ u^1_{z,N}-u^0_{z,N}\approx\Delta z\,G,\ \Delta z(m),\ G\left(\frac{m/s}{m}\right)$$

231 The tridiagonal matrix notation of Eqs.(15a-g), NWFE in z-direction is given in Eq.(16a) as

$$\begin{bmatrix}2\theta\left(\xi_{x,1}+\xi_{y,1}\right) & -\theta\left(-1+\xi_{x,1}+\xi_{y,1}\right) & 0 & 0 & 0\\ -\theta\left(1+\xi_{x,2}+\xi_{y,2}\right) & 2\theta\left(\xi_{x,2}+\xi_{y,2}\right) & \ddots & 0 & 0\\ 0 & -\theta\left(-1+\xi_{x,3}+\xi_{y,3}\right) & \ddots & -\theta\left(-1+\xi_{x,N-3}+\xi_{y,N-3}\right) & 0\\ 0 & 0 & \ddots & 2\theta\left(\xi_{x,N-2}+\xi_{y,N-2}\right) & -\theta\left(-1+\xi_{x,N-2}+\xi_{y,N-2}\right)\\ 0 & 0 & 0 & -\theta\left(1+\xi_{x,N-1}+\xi_{y,N-1}\right) & 2\theta\left(\xi_{x,N-1}+\xi_{y,N-1}\right)\end{bmatrix}\begin{bmatrix}u^1_{Z,1}\\ u^1_{Z,2}\\ \vdots\\ u^1_{Z,N-2}\\ u^1_{Z,N-1}\end{bmatrix}=\begin{bmatrix}f_{z,1}\\ f_{z,2}\\ \vdots\\ f_{z,N-2}\\ f_{z,N-1}\end{bmatrix} \tag{16a}$$

Similarly, the tridiagonal matrix of the percentage power gain, $p_z(\%)$ is given in Eq. (16b)

$$\begin{bmatrix} 2\theta\left(\xi_{x,1}+\xi_{y,1}\right) & -\theta\left(-1+\xi_{x,1}+\xi_{y,1}\right) & 0 & 0 & 0 \\ -\theta\left(1+\xi_{x,2}+\xi_{y,2}\right) & 2\theta\left(\xi_{x,2}+\xi_{y,2}\right) & \ddots & 0 & 0 \\ 0 & -\theta\left(-1+\xi_{x,3}+\xi_{y,3}\right) & \ddots & -\theta\left(-1+\xi_{x,N-3}+\xi_{y,N-3}\right) & 0 \\ 0 & 0 & \ddots & 2\theta\left(\xi_{x,N-2}+\xi_{y,N-2}\right) & -\theta\left(-1+\xi_{x,N-2}+\xi_{y,N-2}\right) \\ 0 & 0 & 0 & -\theta\left(1+\xi_{x,N-1}+\xi_{y,N-1}\right) & 2\theta\left(\xi_{x,N-1}+\xi_{y,N-1}\right) \end{bmatrix} \begin{bmatrix} p^1_{Z,1} \\ p^1_{Z,2} \\ \vdots \\ p^1_{Z,N-2} \\ p^1_{Z,N-1} \end{bmatrix} = \begin{bmatrix} f'_{z,1} \\ f'_{z,2} \\ \vdots \\ f'_{z,N-2} \\ f'_{z,N-1} \end{bmatrix} \tag{16b}$$

The kinematic viscosity, $\upsilon(m^2/s)$ is defined by Nnamchi et al (2019) in Eq.(17) as

$$\upsilon = \frac{1.03\times10^{-06} + 7.0\times10^{-08}T_z - 4\times10^{-11}T_z^2}{2.1313 - 0.003T_z} \qquad \exists \qquad T(K) \tag{17}$$

Temperature variation from the surface to the top of the troposphere, $T_z(K)$ is defined in Eq.(18) according to https://www.weather.gov/jetstream/laye data

$$T_z = T_{surface} + \frac{\left(T_{top} - T_{surface}\right)\left(h_z - h_{surface}\right)}{\left(h_{top} - h_{surface}\right)} \quad \exists \quad T(K),\ h(m), \quad T_{top} = 222.15\,K, T_{surface} = 290.15\,K, \\ h_{top} = 18000\,m,\ h_{surface} = 0.0\,m,\ h_z = h_{Altitude} - h_{Elevation} \tag{18}$$

where $T(K)$ is the temperature, $h\ (m)$ is the height above ground level.

3.0 RESULTS AND DISCUSSION

3.1 Results

The results are presented in both tables and figures. Table 1 shows wind speed boundary conditions at ground level for Eqs. (9a and 16a) and Eqs. (9b and 16b), defining the wind speed and percentage of solar power gain at ground level (depressed station, tropospheric height is zero). Tables 2-4 present the solar power measured results for the elevated (above ground level) station 1 (Engineering Complex), station 2 (Hostel Complex) and station 3 (Library Complex), respectively. In addition, Tables 2-4 present the solar power measured results for the depressed (ground level) station 1 (Engineering Complex), station 2 (Hostel Complex) and station 3 (Library Complex), respectively. The simulation of percentage of solar power gain was limited to altitude of 9200 km^2 with a corresponding wind speed of 42 m/s. The tropospheric height is the difference between the altitude and the elevation of the study areas. Towards the second circling in the radiosonde, the wind speed decreased drastically to zero before rising again. Thus, the altitudes with decreasing to zero wind speed were neglected in this analysis as the effect of wind speed diminished and later vanished.

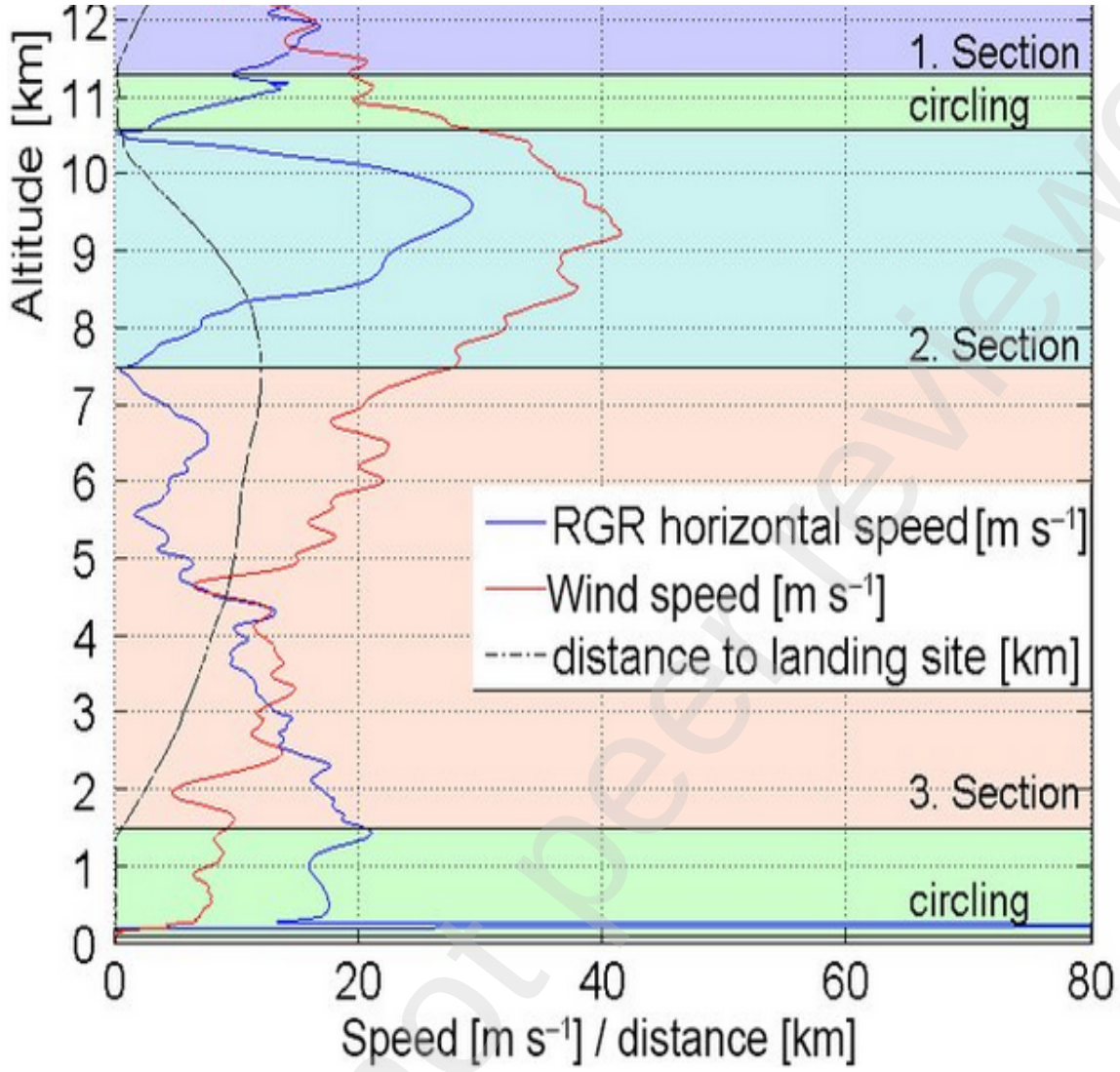

Fig. 3. Altitude versus wind speed based on radiosonde (Kräuchi and Philipona, 2016)

252

253 **Table 1.**

254 Natural wind flow and percentage power gain boundary conditions for the study areas

Study area	Dimension (km)	Wind speed boundary condition (m/s)	Percentage power gain boundary condition (-)
NR	$x = y = z = 0$	$u_x = u_y = u_z = 0$	$p_z = 0$
ER	$x = y = z = 0$	$u_x = u_y = u_z = 0$	$p_z = 0$
CR	$x = y = z = 0$	$u_x = u_y = u_z = 0$	$p_z = 0$
WR	$x = y = z = 0$	$u_x = u_y = u_z = 0$	$p_z = 0$

255

256

Table 2

Measured average data at station 1 (Engineering Complex at Kampala International University, WC)

Parameter	Local time (pm)									
	Elevated station					Depressed or ground station				
	1:00	1:15	1:30	1:45	2:00	1:00	1:15	1:30	1:45	2:00
Tropospheric height, h_z(m)	19.26	19.26	19.26	19.26	19.26	0	0	0	0	0
Wind speed, u_z (m/s)	2.50	2.64	2.68	2.54	2.66	0	0	0	0	0
Short circuit current, I(A)	0.24	0.53	0.56	0.58	0.58	0.23	0.51	0.54	0.56	0.56
Open circuit voltage, V(V)	21	21	21	21	21	21	21	21	21	21
Measured power, P_z (W)	4.94	11.13	11.76	12.18	12.18	4.75	10.72	11.32	11.74	11.73
Measured percentage power gain, $p_{measured}$(%)	0.038	0.038	0.039	0.038	0.038	0	0	0	0	0
Simulated percentage power gain, $p_{simulated}$(%	0.037	0.039	0.040	0.038	0.040	0	0	0	0	0
Root mean square error, RMSE	0.001									

Table 3

Measured average data at station 2 (Hostel Complex of Kampala International University, WC)

Parameter	Local time (pm)									
	Elevated station					Depressed or ground station				
	1:00	1:15	1:30	1:45	2:00	1:00	1:15	1:30	1:45	2:00
Tropospheric height, h_z(m)	37.65	37.65	37.65	37.65	37.65	0	0	0	0	0
Wind speed, u_z(m/s)	2.66	2.64	2.79	2.63	2.60	0	0	0	0	0
Short circuit current, I(A)	0.34	0.37	0.44	0.50	0.53	0.32	0.35	0.38	0.48	0.49
Open circuit voltage, V(V)	20.27	21.80	20.00	20.72	20.05	20.11	21.69	21.51	20.61	20.18
Measured power, P_z (W)	6.95	8.10	8.70	10.45	10.65	6.48	7.59	8.17	9.89	9.89
Measured percentage power gain, $p_{measured}$(%)	0.074	0.07	0.07	0.06	0.08	0	0	0	0	0
Simulated percentage power gain, $p_{simulated}$(%)	0.075	0.067	0.094	0.057	0.087	0	0	0	0	0
Root mean square error, RMSE	0.014									

Table 4

Measured average data at station 3 (Library Complex of Kampala International University, WC)

Parameter	Local time (pm)									
	Elevated station					Depressed or ground station				
	1:00	1:15	1:30	1:45	2:00	1:00	1:15	1:30	1:45	2:00
Tropospheric height, h_z(m)	77.7	77.7	77.7	77.7	77.7	0	0	0	0	0
Wind speed, u_z(m/s)	2.69	2.75	2.67	2.75	2.74	0	0	0	0	0
Short circuit current, I(A)	0.53	0.57	0.57	0.53	0.49	0.25	0.24	0.24	0.23	0.23
Open circuit voltage, V(V)	22	21	20	21	22	21	21	21	21	21
Measured power P_z (-)	11.56	11.78	11.48	11.22	10.75	10.08	10.33	9.98	9.84	9.42
Measured percentage power gain $p_{simulated}$(%)	0.15	0.14	0.15	0.14	0.14	0	0	0	0	0
Simulated percentage power gain $p_{simulated}$(%)	0.15	0.14	0.15	0.14	0.14	0	0	0	0	0
Root mean square error, RMSE	0.005									

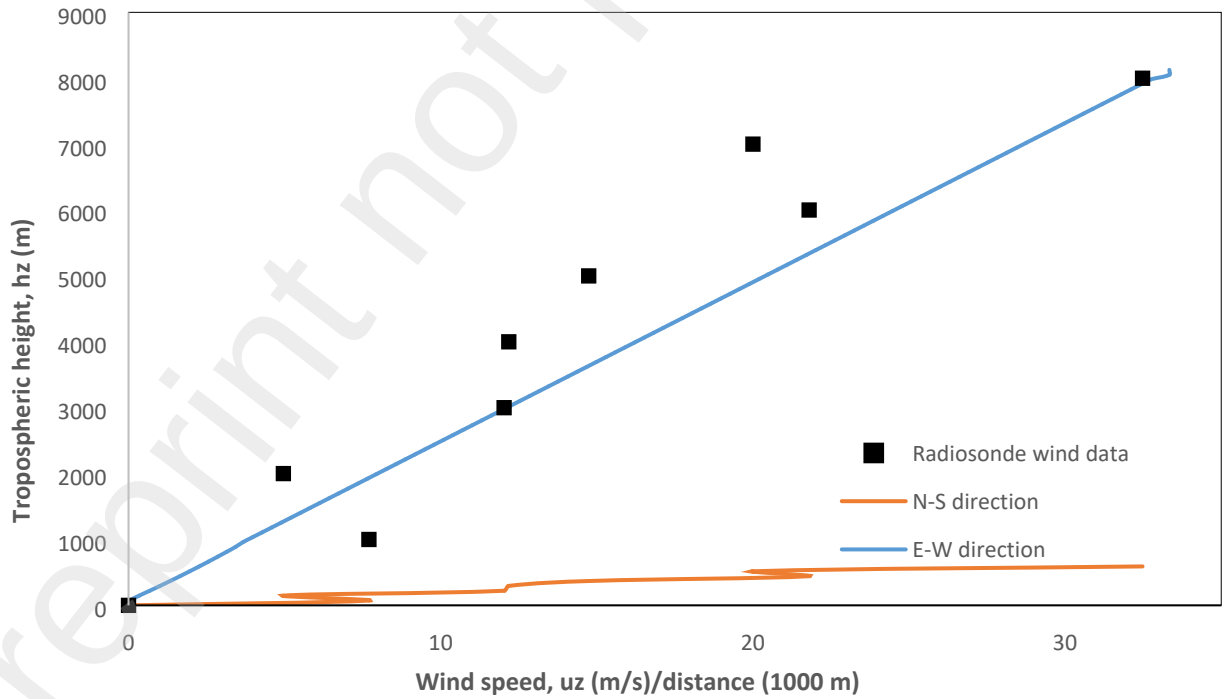

Fig. 4 Growth of tropospheric height with the wind speed for the Northern Region.

Figures 4-7 portray fitted line graph of troposphere Height against the wind speed for NR, ER, CR and WR, respectively. Similarly, Figures 8-11 portray simple line graph of wind speed against the percentage of solar power gain for NR, ER, CR and WR, respectively. Whereas Figs. (12-15) give the composite or contour plot of Percentage of solar power gain against tropospheric Height and the wind speed. These results are germane for discussion and drawing apt conclusions.

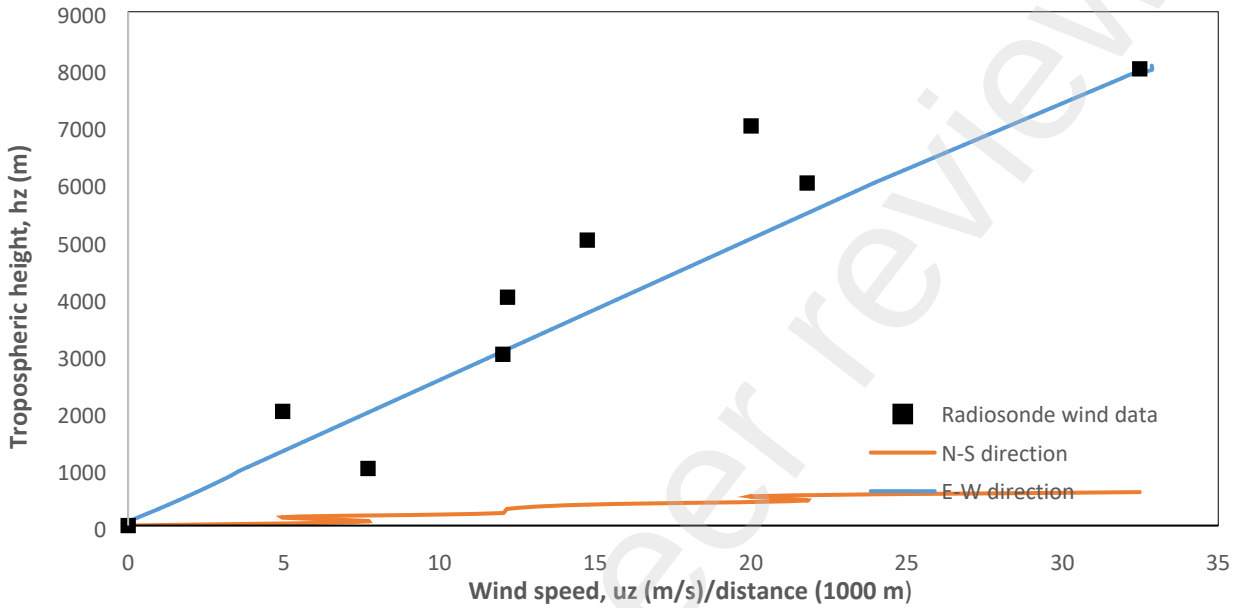

Fig. 5 Reliance of tropospheric height on the wind speed for the Eastern Region.

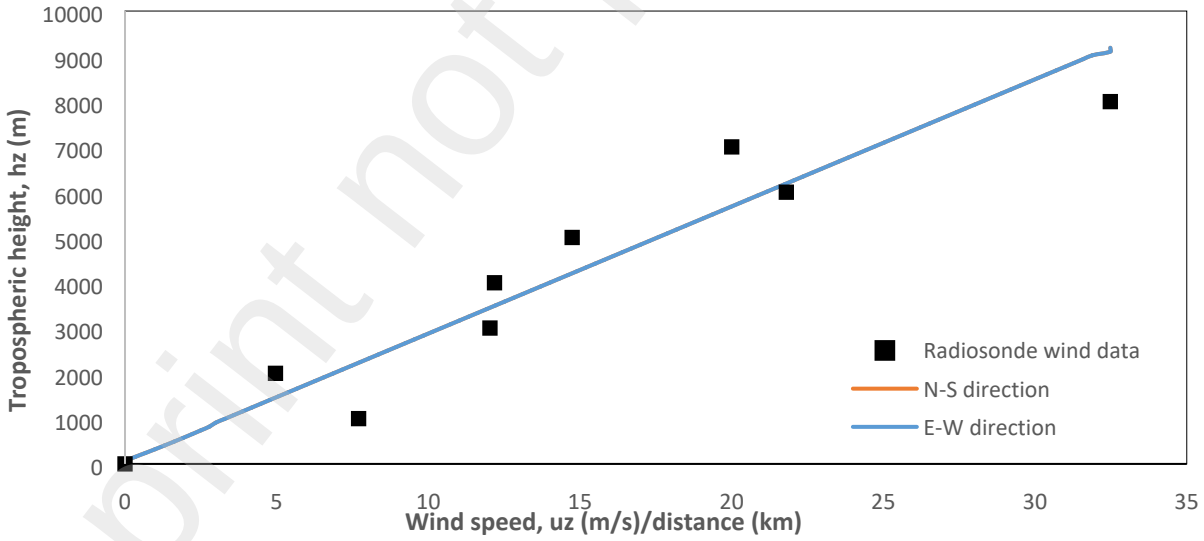

Fig. 6. Dependence of tropospheric height on the wind speed for the Central Region.

3.2 Discussion

The results are discussed according to the three cardinal objectives of the study; establishment of the functional relationship between the tropospheric height and the wind speed, formulation of the functional

relationship between the tropospheric height and percentage of power gain, and lastly unification of the three parameters (percentage of solar power gain, tropospheric Height and wind speed) in contour for the study areas.

3.2.1 Functional relationship between tropospheric Height and the wind speed

Figures 4-7 demonstration the linear behavior between the tropospheric height and the wind speed for the study areas (Figs. 1 and 2). This result supports that Eq. (9a) is a linear partial derivative model of NWFE because the body or external forces were not considered in their formulations, however, it describes the linear relation between wind speed and tropospheric height. Despite the radiosonde data in Fig. 3 showed a wavy curve between the altitude and the wind speed. The tropospheric height is derived from the radiosonde by subtracting the elevation of the study areas from the altitude. The radiosonde measured data fairly fitted well with the simulated results in Figs. 4-7, the agreement supports the implementation of simulated results in this work. In addition, above the ground level, the influence of topography becomes insignificant, thus, the wind speed data in both north south and east-west directions cluster as shown in Figs. 4-7. Significant wind speed of approximately 33 and 42 ms^{-1}/distance 1000 m correspond to tropospheric heights of 8100 and 9200 m, respectively, these wind speeds are very good for wind farm operations provided a stack of these heights are available.

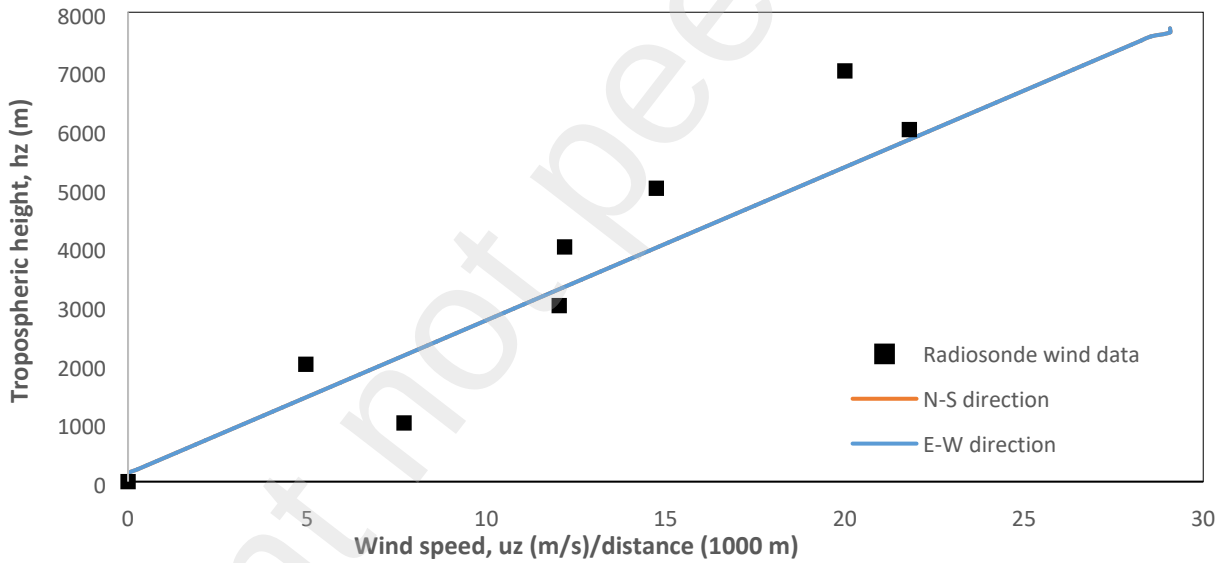

Fig. 7. Variation of tropospheric height with the wind speed for the Western Region.

3.2.2 Functional relationship between tropospheric height and percentage power gain

Figures 8-11 display the linear behavior between the percentage of solar power gain and the tropospheric height for the study areas in Figs. 1 and 2. Similarly, these results support that Eq. (9b) is a linear partial derivative model of NWFE because the body or external forces as earlier mentioned were not considered in their formulations, nevertheless, it defines the linear relationship between the percentage of solar power gain and tropospheric height. In addition, above the ground level, the influence of topography becomes unimportant, as the percentage of solar power gain in both north south and east west directions cluster as shown in Figs. 8-11. Figures 8-11 could not be fitted because measurements could not be carried in the high tropospheric height. However, Tables 2-4 shows practical measurement of the percentage of solar power

gain, the measurements are conducted close to ground level in three elevated stations in Fig. 2. The root mean square error (RMSE) analysis of simulated and measured results gave 0.001, 0.014, 0.005 in Tables 2-4, respectively. The variation in RMSE could be attributed to changes in experimental conditions as the measurement were carried out on different days in different stations. Above the tropospheric height, of 9200 m, the wind speed diminished to zero, thus, a maximum tropospheric of 9200 m was considered in this work since wind speed is defined from ground level to this height (9200 m).

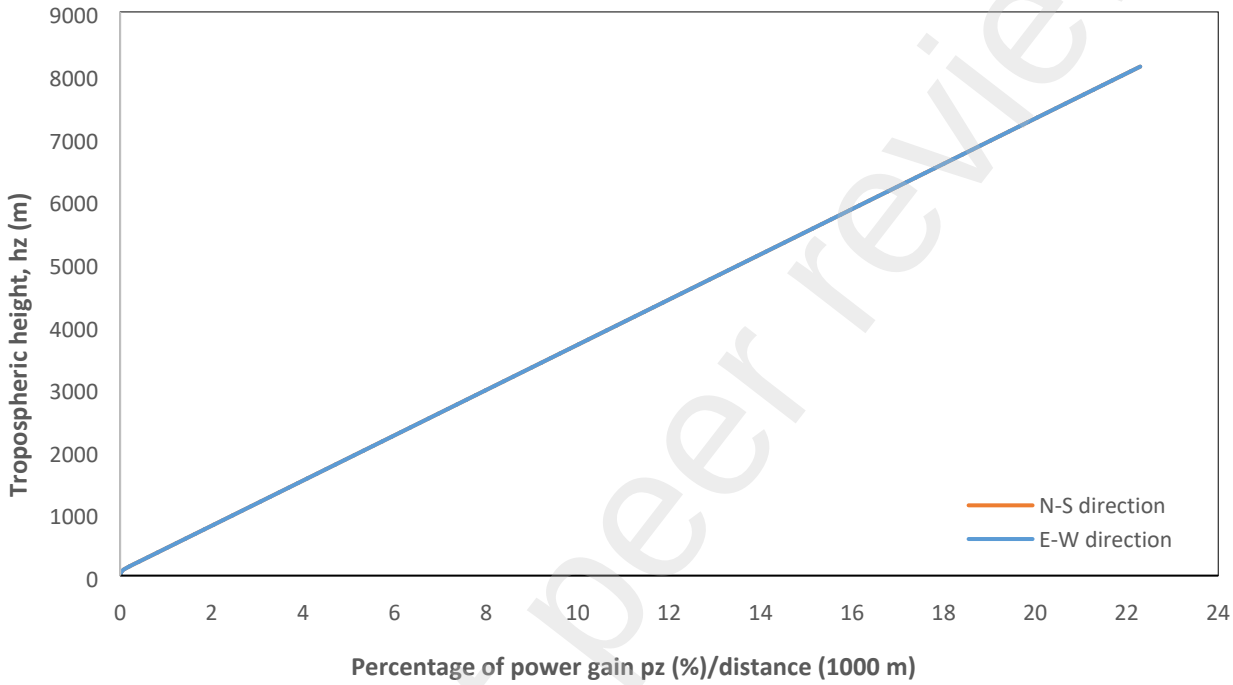

Fig. 8. Growth of tropospheric height with the percentage of solar power gain for the Northern Region.

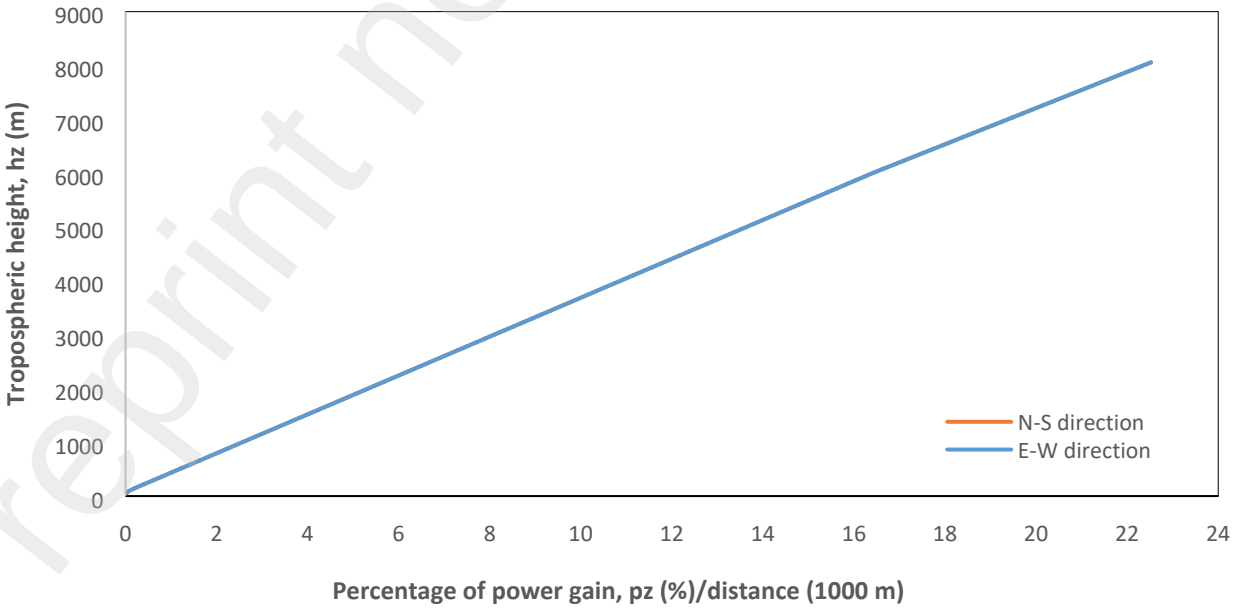

Fig. 9. Impact of tropospheric height on the percentage of solar power gain for the Eastern Region.

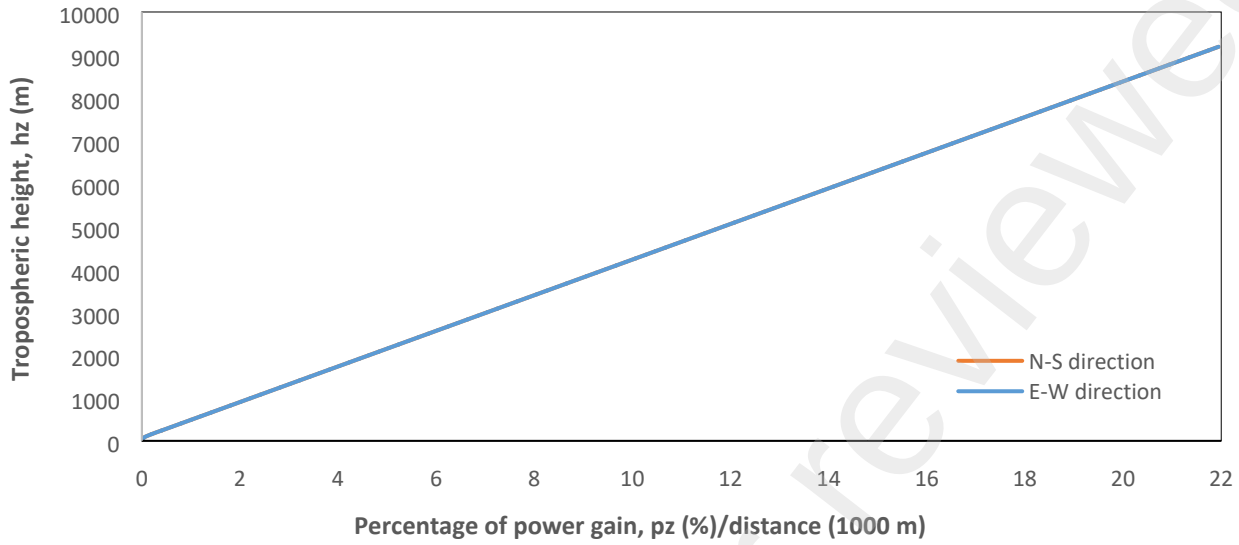

Fig. 10. Influence of tropospheric height on the percentage of solar power gain for the Central Region.

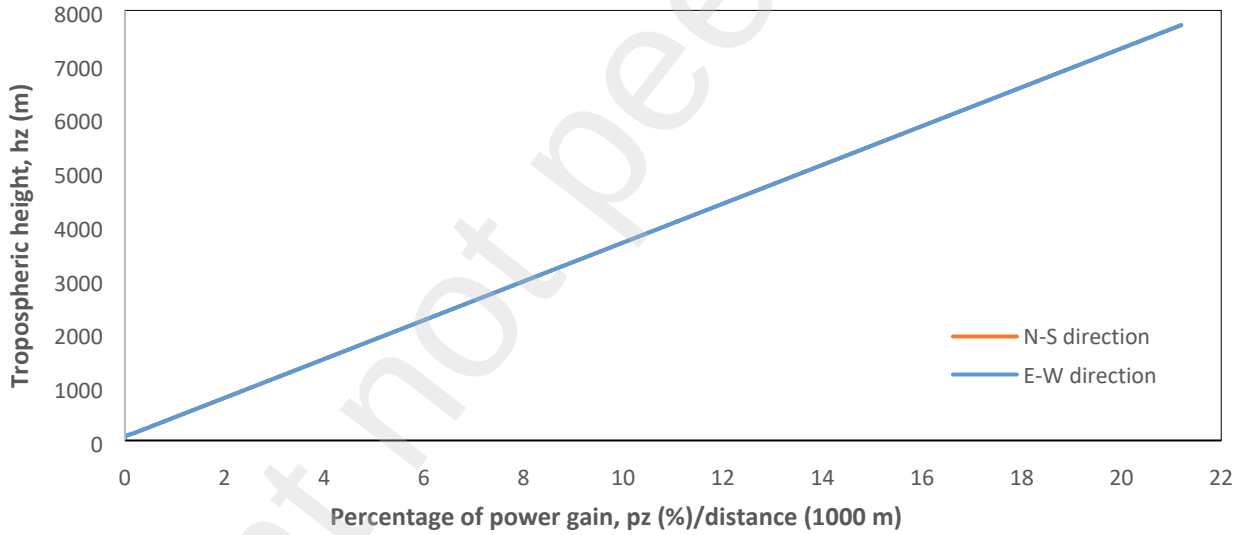

Fig. 11. Effect of tropospheric height on the percentage of solar power gain for the Western Region.

3.2.3 Composite behavior of Percentage of solar power gain with tropospheric Height and wind speed

The percentage of solar power gain was simulated in space where both the tropospheric height and the wind speed are defined. The composite behavior of percentage of solar power gain yielded the contour plots in Figs. 12-15 for NR, ER, CR and WR, respectively. Remarkable the percentage of solar power gain isolines shows the range of tropospheric heights and wind velocity that support such percentage solar power gain. It obvious that from ground level to approximately 1000 m that small percentage of solar power gain of 2 % is possible to attain. This micro percentage of solar power gain of 0.038, 0.071 and 0.144 % were measured and computed at stations; 1, 2 and 3 respectively. The corresponding RMSE (0.001, 0.014, 0.005) obtained in Tables 2-4 is quite low. Low percentage of solar power gain results are supported by Amusan

and Igbudu (2014), but comparing the percentage of solar power gain by Panjwani and Narejo (2014), who assert range values of 7 to 12%, at tropospheric heights of 0.243 m it is practically impossible to gain such considering the closes significant percentage of solar power gain at approximately height of 1000 m is 2%. Experiment and simulation backed up the present result; hence, the percentage of solar power gain of 2% is quite realistic. Further comparison of the present results with that of Chitturi et al (2018) claimed percentage of solar power gain of 42% height of 1764 m, however, the present work supports about 4% solar power gain. The erroneous generation of Amusan and Igbudu (2014) on insignificant percentage of solar power gain from the earth to the sun is spurious as the present work shows approximately 20 % solar power gain in Figs. 12-15. The prospect of having percentage of solar power gain above 20 % is possible by using High Altitude Platforms, HAP (either lighter than air or heavier than air). The present work demystifies the false claims of attaining a high percentage of solar power gain near ground level is practically impossible. However, the prospect of achieving high percentage of solar power gain is possible on the application of HAPs (Aglietti et al, 2008; Gupta et al, 2019). Moreover, it is obvious that high wind speed is attained at high altitude or tropospheric height where air temperature is quite low, this condition accounts for high percentage of solar power gain (Hassan et al., 2021; Deokar et al, 2021; Dwivedi, 2020), passive (Ramkiran et al., 2021; Rakino et al., 2019, Wu and Xiong, 2014). The percentage of solar power gain is independent of size and number of solar panel used, but measured power is dependent on the size and number of solar panel. Notably, above ground level energy exploitation is possible with the application of HAPs. Besides, the results in Figs. 12-15 are almost similar, indicates that this result could be used anywhere, provided the elevation is subtracted from the altitude (9200 m) to obtain the tropospheric. The tropospheric height will unveil the possible percentage of solar power gain. Thus, the application of the results goes beyond the present study areas.

Lastly, the economic analysis of acquiring HAP is out of the scope of this work, however, it is technically sound but costly to acquire the HAP.

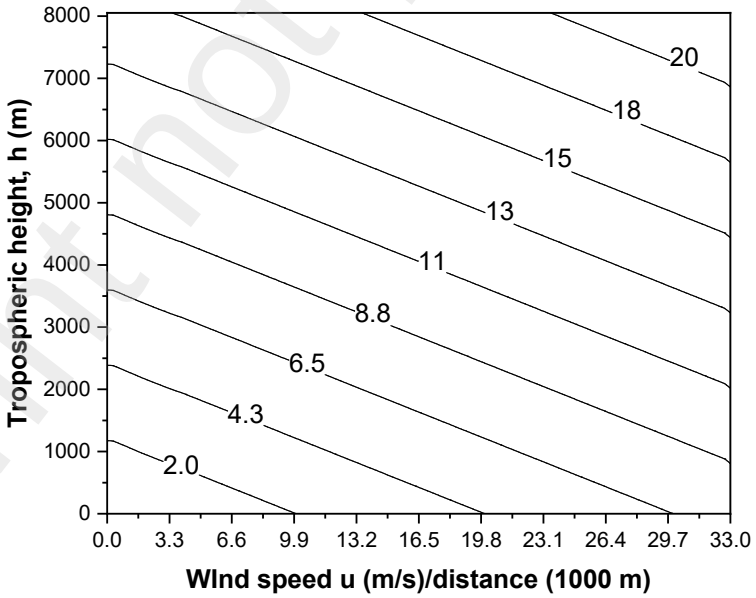

Fig. 12. Response of the percentage of solar power gain, $p(\%)$ to tropospheric height and wind speed for the Northern Region.

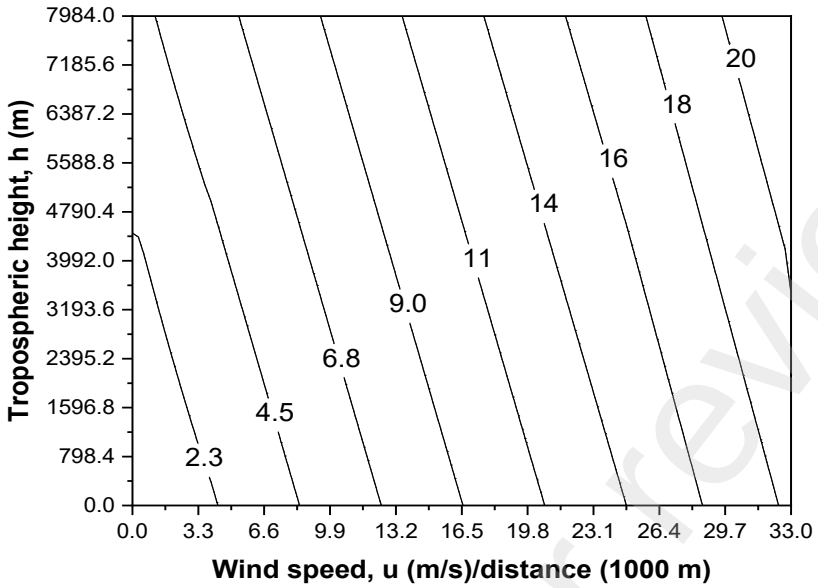

Fig. 13. Response of the percentage of solar power gain, $p(\%)$ to tropospheric height and wind speed for the Eastern Region.

348

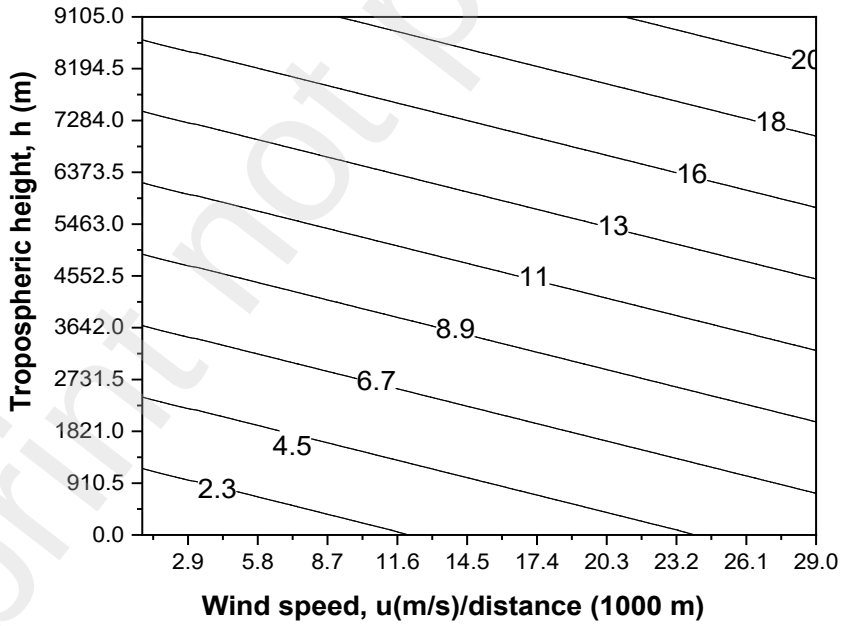

Fig. 14. Reaction of the percentage of solar power gain, $p(\%)$ to tropospheric height and wind speed for the Central Region.

349

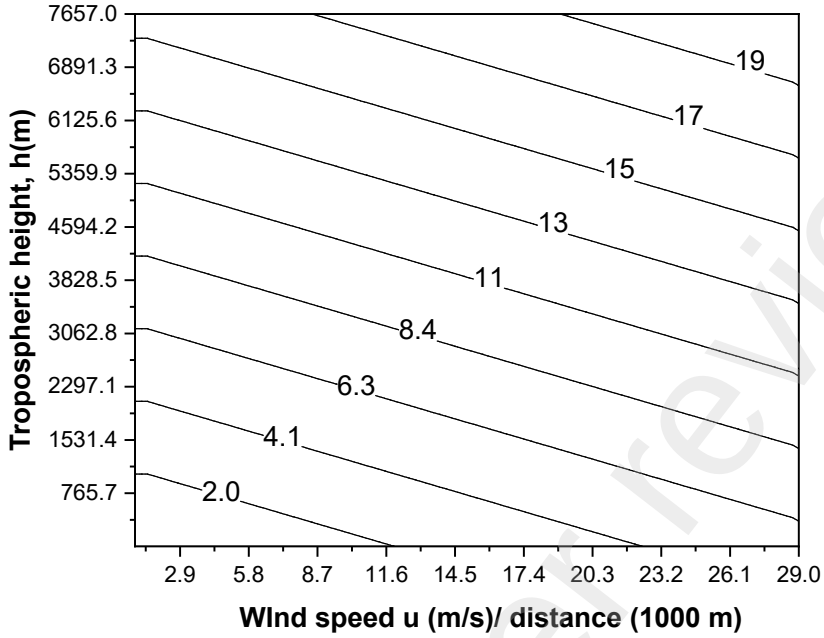

Fig. 15. Response of the percentage of solar power gain, $p(\%)$ to tropospheric height and wind speed for the Western Region.

4.0 CONCLUSIONS

This research has accomplished energy exploration above the ground level via modeling and simulations, and experiments. This research is necessitated in bid to explore energy above the ground level for areas not favored with ground platform in generation of solar power into electricity. The study reveals that near ground level, about 1000 m could attract percentage of solar power gain of 2 %, but at high altitude of 9200 m, the percentage of solar power gain is prominent to the tune of 20 %, however, at altitudes above 9200 m more percentage of solar power gain is possible to achieve.

The model simulation indicated a linear relationship between the tropospheric height and the wind speed. Similarly, a linear relationship exists between the tropospheric height and the percentage of solar power gain. The linear relationship further reveals that the natural wind flow equation, NWFE is a linear partial derivative model, describing the potentials; wind speed and the percentage of solar power gain in space with appropriate boundary conditions in three dimensions.

The major results, presenting the percentage of solar power gain as a function of tropospheric height and wind speed are vast in their applications. Outside the study areas, the results are applicable to other study areas having the same elevation as Uganda (1100 m above sea level). Moreover, the application of the results could extend beyond equal elevation; any geographical area having elevation below 1100 m could conveniently use these results to estimate possible percentage of solar power gain by subtracting its elevation from 9200 m. Pertinently, accessing more percentage of solar power gain entails the application of high-altitude platforms (either light-than-air or heavier-than-air), this technology overshadows the influence of topography and other related factors that hinder full access to solar irradiance by ground platforms.

ACKNOWLEDGEMENT

The authors appreciate Kräuchi and Philipona (2016) for making Radiosonde data available for the study and the rest of authors featured in the literature.

CONFLICT OF INTERESTS

Authors wish to declare that there is no conflict of interests of any kind.

FUNDING

Authors wish to declare that institution or governmental body sponsored this research.

DATA AVAILABILITY

There is no data availability associated to this manuscript

REFERENCES

1. AccuWeather, Ishaka, Bushenyi, Average wind speed. https://www.accuweather.com/en/ug/ishaka/1895309/current-weather/1895309. (Accessed: 10 May, 2022).
2. Aglietti, G. S., Markvart, T., Tatnall, A. R., & Walker, S. J. (2008). Solar power generation using high altitude platforms feasibility and viability. Progress in Photovoltaics: Research and Applications, 16(4), 349
3. Ahammad, M. J., Rahman, M. A., Alam, J., & Butt, S. (2019). A computational fluid dynamics investigation of the flow behavior near a wellbore using three-dimensional Navier–Stokes equations. Advances in Mechanical Engineering, 11(9), 1687814019873250. https://doi.org/10.1177/1687814019873250.
4. Alrwashdeh, S. S. (2018). The effect of solar tower height on its energy output at Ma'an-Jordan. AIMS Energy, 6(6), 959-966.
5. Amusan, J. A., & Igbudu, O. (2014). The effect of pole's height on the output performance of solar power system. Scientia Africana, 13(2).
6. Asgharzadeh, A., Marion, B., Deline, C., Hansen, C., Stein, J. S., & Toor, F. (2018). A sensitivity study of the impact of installation parameters and system configuration on the performance of bifacial PV arrays. IEEE Journal of Photovoltaics, 8(3), 798-805.
7. Atkin, P., & Farid, M. M. (2015). Improving the efficiency of photovoltaic cells using PCM infused graphite and aluminium fins. Solar Energy, 114, 217-228.
8. Bhattacharya, T., Chakraborty, A. K., & Pal, K. (2014). Effects of ambient temperature and wind speed on performance of monocrystalline solar photovoltaic module in Tripura, India. Journal of Solar Energy, Volume 2014 |Article ID 817078 | https://doi.org/10.1155/2014/817078.
9. Bishoge, O. K., Zhang, L., & Mushi, W. G. (2018). The potential renewable energy for sustainable development in Tanzania: A review. Clean Technologies, 1(1), 70-88. https://doi.org/10.3390/cleantechnol1010006.

10. Blumthaler, M., Ambach, W., & Ellinger, R. (1997). Increase in solar UV radiation with altitude. Journal of photochemistry and Photobiology B: Biology, 39(2), 130-134. https://doi.org/10.1016/s1011-1344(96)00018-8.
11. Bogdanov, D., Ram, M., Aghahosseini, A., Gulagi, A., Oyewo, A. S., Child, M., ... & Breyer, C. (2021). Low-cost renewable electricity as the key driver of the global energy transition towards sustainability. Energy, 227, 120467. https://doi.org/10.1016/j.energy.2021.120467.
12. Burmasheva, N., & Prosviryakov, E. (2022). Exact Solutions to Navier–Stokes Equations Describing a Gradient Nonuniform Unidirectional Vertical Vortex Fluid Flow. Dynamics, 2(2), 175-186. https://doi.org/10.3390/dynamics2020009.
13. Chandra, S., Agrawal, S., & Chauhan, D. S. (2018). Effect of ambient temperature and wind speed on performance ratio of polycrystalline solar photovoltaic module: An experimental analysis. International Energy Journal, 18(2): 171-180.
14. Chitturi, S. R. P., Sharma, E., & Elmenreich, W. (2018, June). Efficiency of photovoltaic systems in mountainous areas. In 2018 IEEE International Energy Conference (ENERGYCON) (pp. 1-6). IEEE.
15. Deokar, V. H., Bindu, R. S., & Potdar, S. S. (2021). Active cooling system for efficiency improvement of PV panel and utilization of waste-recovered heat for hygienic drying of onion flakes. Journal of Materials Science: Materials in Electronics, 32(2), 2088-2102. https://doi.org/10.1007/s10854-020-04975-3
16. Dwivedi, P., Sudhakar, K., Soni, A., Solomin, E., & Kirpichnikova, I. (2020). Advanced cooling techniques of PV modules: A state of art. Case studies in thermal engineering, 21, 100674. https://doi.org/10.1016/j.csite.2020.100674.
17. Gupta, Sowmya; Duttagupta, Siddhartha P.; Vachhani, Leena; Mitra, Mira (2019). Attitude control of LTA platform for generation of a non-oscillatory solar power. Solar Energy, 189(), 131–150. https://doi.org/10.1016/j.solener.2019.07.017 -359.
18. Hasan, A., Sarwar, J., Alnoman, H., Abdelbaqi, S. (2017) Yearly energy performance of a photovoltaic-phase change material (PV-PCM) system in hot climate. Sol Energy 146:417–429. https://doi.org/10.1016/j.solener.2017.01.070.
19. Hassan H, Yousef SM, Abo-Elfadl S (2021) Energy, exergy, economic and environmental assessment of double pass V-corrugated-perforated finned solar air heater at different air mass ratios. Sustain Energy Technol Assessments 43:100936. https://doi.org/10.1016/j.seta.2020.100936
20. jntechenergy.com. Are Solar Panels More Efficient At High Altitude? https://www.conserve-energy-future.com/are-solar-panels-efficient-at-high-altitude.php (accessed 7/9/2022).
21. Klemen Zakšek; Tomaž Podobnikar; Krištof Oštir (2005). Solar radiation modelling., Computers & Geosciences 31(2), 233–240. https://doi.org/10.1016/j.cageo.2004.09.018.
22. Kräuchi, A., & Philipona, R. (2016). Return glider radiosonde for in situ upper-air research measurements. Atmospheric Measurement Techniques, 9(6), 2535-2544.
23. Lee, S., Ryi, S. K., & Lim, H. (2017). Solutions of Navier-Stokes equation with Coriolis force. Advances in Mathematical Physics, 2017. https://doi.org/10.1155/2017/704268.
24. Loria, A. F. R. (2020). Energy geostructures: Theory and application. In E3S Web of Conferences (Vol. 205, p. 01004). EDP Sciences.
25. Luo, Z., Huang, Z., Xie, N., Gao, X., Xu, T., Fang, Y., & Zhang, Z. (2017). Numerical and experimental study on temperature control of solar panels with form-stable paraffin/expanded graphite composite PCM. Energy Conversion and Management, 149, 416-423.

26. Mahdi, J. M., Singh, R. P., Al-Najjar, H. M. T., Singh, S., & Nsofor, E. C. (2021). Efficient thermal management of the photovoltaic/phase change material system with innovative exterior metal-foam layer. Solar Energy, 216, 411-427. https://doi.org/10.1016/j.solener.2021.01.008.
27. Majid, M. A. (2020). Renewable energy for sustainable development in India: current status, future prospects, challenges, employment, and investment opportunities. Energy, Sustainability and Society, 10(1), 1-36.
28. Maka, A. O., & Alabid, J. M. (2022). Solar energy technology and its roles in sustainable development. Clean Energy, 6(3), 476-483. https://doi.org/10.1093/ce/zkac023.
29. Martinez-Gracia, Amaya (2019). Solar Hydrogen Production || Solar energy availability, (), 113–149. https://doi.org/10.1016/B978-0-12-814853-2.00005-9.
30. Mundu, M. M., Nnamchi, S. N., Ukagwu, K. J., Peter, B. A., Nnamchi, O. A., & Ssempewo, J. I. (2022). Numerical modelling of wind flow for solar power generation in a case study of the tropical zones. Modeling Earth Systems and Environment, 1-12. https://doi.org/10.1007/s40808-021-01343-w.
31. Nnamchi, S. N., Nnamchi, O. A., S. Odebiyi, O., Edosa, O. O., & Wanazusi, T. (2019). Experimental verification of suitability of insulation testing rig in determining thermophysical properties of insulating materials. Cogent Engineering, 6(1), 1657264.
32. Nnamchi, O. A., Ndukwu, M. C., & Nnamchi, S. N. (2021). Modelling and simulation of multi-coupled heat and mass transfer processes: A case study of solar biomass dryer. Thermal Science and Engineering Progress, 25, 101007. https://doi.org/10.1016/j.tsep.2021.101007.
33. Nnamchi, S. N., Mundu, M. M., Nnamchi, O. A., Onochie, U., & Jagun, Z. O. (2022). Differential modelling and simulation of solar power potential: a helio-application of biharmonic model. Modeling Earth Systems and Environment, 8(2), 2383-2400. https://doi.org/10.1007/s40808-021-01232-2.
34. Oko, C. O. C., & Nnamchi, S. N. (2013). Coupled heat and mass transfer in a solar grain dryer. Drying Technology, 31(1), 82-90. https://doi.org/10.1080/07373937.2012.719561.
35. Osma, G., Ordóñez, G., Hernández, E., Quintero, L., & Torres, M. (2016). The impact of height installation on the performance of PV panels integrated into a green roof in tropical conditions (Vol. 205, pp. 147-156). Southampton, UK: WIT Press.
36. Owusu, P. A., & Asumadu-Sarkodie, S. (2016). A review of renewable energy sources, sustainability issues and climate change mitigation. Cogent Engineering, 3(1), 1167990. https://doi.org/10.1080/23311916.2016.1167990.
37. Pielke Sr, R. A. (2013). Mesoscale meteorological modeling. Academic press.
38. Radwan, A. G., Khanday, F. A., & Said, L. A. (Eds.). (2021). Fractional-Order Modeling of Dynamic Systems with Applications in Optimization, Signal Processing, and Control. Academic Press.
39. Rakino, S. A., Suherman, S., Hasan, S., & Rambe, A. H. (2019, November). A Passive Cooling System for Increasing Efficiency of Solar Panel Output. In Journal of Physics: Conference Series (Vol. 1373, No. 1, p. 012017). IOP Publishing. https://doi.org/10.1088/1742-6596/1373/1/012017.
40. Ramkiran, B., Sundarabalan, C. K., & Sudhakar, K. (2021). Sustainable passive cooling strategy for PV module: A comparative analysis. Case Studies in Thermal Engineering, 27, 101317. https://doi.org/10.1016/j.csite.2021.101317.
41. Rapp, B. E. (2016). Microfluidics: modeling, mechanics and mathematics. William Andrew.
42. Rublev, G., Bogdanova, L., Kurbatova, S., Krasnousov, S., & Kolmakov, V. (2021). Socio-economic model of sustainable development. In E3S Web of Conferences (Vol. 244, p. 10053). EDP Sciences.

43. Sahu, P. P., Swain, A., & Sarangi, R. K. (2021). Role of PCM in solar photovoltaic cooling: An overview. In Proceedings of International Conference on Thermofluids (pp. 245-259). Springer, Singapore.
44. Seto, D. B., Kristiawan, B., & Arifin, Z. (2021, March). Solar Cell Cooling with Phase Change Material (PCM) for Enhanced Efficiency: A Review. In IOP Conference Series: Materials Science and Engineering (Vol. 1096, No. 1, p. 012052). IOP Publishing. https://iopscience.iop.org/article/10.1088/1757-899X/1096/1/012052.
45. Shastry, D. M. C., & Arunachala, U. C. (2020) Thermal management of photovoltaic module with metal matrix embedded PCM. J Energy Storage 28:101312. https://doi.org/10.1016/j.est.2020.101312.
46. Taha, H. E., & Gonzalez, C. (2022). What does nature minimize in every incompressible flow. arXiv preprint arXiv:2112.12261. https://doi.org/10.48550/arXiv.2112.12261.
47. Thadani, H. L., & Go, Y. I. (2021). Integration of solar energy into low-cost housing for sustainable development: case study in developing countries. Heliyon, 7(12). https://doi.org/10.1016/j.heliyon.2021.e08513.
48. Tucho, G. T., & Kumsa, D. M. (2020). Challenges of achieving sustainable development Goal 7 From the perspectives of access to modern cooking energy in developing countries. Frontiers in Energy Research, 8, 564104.
49. Wu, S., & Xiong, C. (2014). Passive cooling technology for photovoltaic panels for domestic houses. International Journal of Low-Carbon Technologies, 9(2), 118-126.
50. Zhang, L., Zhu, W., Du, H., & Lv, M. (2021). Multidisciplinary design of high altitude airship based on solar energy optimization. Aerospace Science and Technology, 110, 106440. https://doi.org/10.1016/j.ast.2020.106440.